European Journal of Mechanics B/Fluids xxx (2009) 1–12

Contents lists available at ScienceDirect

European Journal of Mechanics B/Fluids

journal homepage: www.elsevier.com/locate/ejmflu

An active flow control strategy for the suppression of vortex structures behind a circular cylinder

Sridhar Muddada, B.S.V. Patnaik*

Fluid Mechanics Laboratory, Department of Applied Mechanics, Indian Institute of Technology Madras, Chennai 600 036, India

ARTICLE INFO

Article history:
Received 2 March 2009
Received in revised form
2 November 2009
Accepted 10 November 2009
Available online xxx

Keywords:
Active flow control
Vortex shedding
Circular cylinder
CFD
Fluid flow patterns
Chaos control
Synchronization
Navier - Stokes equations
MSBC

ABSTRACT

An algorithm is proposed to model, predict and control vortex shedding behind a circular cylindrical configuration. The main ingredients of the algorithm include multiple-feedback sensors, actuators (with zero net mass injection) and a control strategy. Along with the mass and momentum conservation equations, a control equation is implemented to enable the desired flow control goals. A number of sensors are chosen in the downstream of the body to report the state of the flow. The role of externally controllable actuators on the fluid flow patterns past a circular configuration is assessed. To enable, zero net mass injection, two simple rotary type mechanical actuators are located at 120°, right behind the main cylinder. The popular finite volume based SIMPLE scheme is employed for the numerical calculations. As a precursor, the scheme simulates flow past an isolated cylinder, which is validated over a moderate range of Reynolds numbers. The design parameters of interest such as Strouhal number, drag and lift coefficients etc are used for the purpose of validation. The simulated flow fields are compared against the flow visualization study, which clearly demonstrates the efficacy of the actuators at discrete levels of rotation. The basic character of the flow is completely modified at $U_c/U_\infty = 2.0$ and $Re = 100$, where a complete suppression of vortex shedding is observed. This is tantamount to complete control of all the global instability modes. Fictitious tracer particles are released to visualize the vortex structures in the form of streaklines. The results clearly demonstrate the effectiveness of a rather simple active control algorithm in suppressing the vortex structures. All the relevant fluid flow features of the bluff-body fluid mechanics under the influence of actuators are studied in the sub-critical Reynolds number range of $Re = 100$–300.

1. Introduction

Understanding and controlling wakes is of paramount scientific and engineering importance. Bluff body wakes have been extensively studied by employing theoretical, numerical and experimental means [1–4]. The wake region formed behind a bluff body (say, the popular circular cylindrical configuration) is complex, as it involves the interaction of three types of shear layers, viz., a boundary-layer, a separating shear-layer and a wake [2]. A wide variety of structures encountered in civil, mechanical and ocean engineering practice can be classified either as bluff or streamlined. Bluff body configurations are not highly desirable, as the form drag of these bodies makes a contribution of roughly two-thirds to the total drag. For a flexibly mounted bluff body, transverse vibrations are induced due to *resonance* or *phase-locking*, when the vortex shedding frequency (f_{vs}) is in the neighborhood of the natural frequency (f_n) of the structure [5,6]. Vortex induced resonance is a well known phenomenon even at low to moderate Reynolds numbers. The challenge lies in controlling these vibrations caused by vortex shedding. At moderate to high Reynolds numbers, the wake region and the boundary-layer are turbulent, such flows encompass a wide spectrum of eddies from Kolmogorov's micro scale to eddies as big as the size of the body, known as the integral scale. Understanding and controlling these eddies of different length scales and time scales is central to achieving energy efficient systems and processes. Although a large body of literature is available, even after over a century of effort by researchers and engineers, the problem of bluff body flow still remains almost entirely in the empirical, descriptive realm of knowledge. These numerical simulations are not just theoretical solutions but experimental ones, parallel to those realized in the laboratory [7].

One of the attempts to control these vortex structures was initiated as early as 1910, by the legendary fluid dynamicist, Ludwig Prandtl, who demonstrated his ship of zero viscous resistance through flow around two counter rotating cylinders [8]. A large number of systematic experiments have been carried out by Modi [9] and his co-workers, who have employed rotating cylinders as an

* Corresponding author. Tel.: +91 44 2257 4068.
E-mail address: bsvp@iitm.ac.in (B.S.V. Patnaik).

0997-7546/$ – see front matter © 2009 Elsevier Masson SAS. All rights reserved.
doi:10.1016/j.euromechflu.2009.11.002

integral part of airfoils, a variety of bluff bodies such as buildings, moving vehicles etc and the concept has been shown to be remarkably effective and successful in delaying separation [9,10]. Since momentum is injected into the shear layers by means of a moving wall (rotating control cylinders), in the literature it is also popularly known as Moving Surface Boundary-layer Control (MSBC), which contributes in most of the following ways [9]:

- It retards the growth of the boundary-layer by minimizing relative motion between the surface and the free stream.
- It injects momentum into the boundary-layer.
- It creates a region of high suction and thereby accelerates the flow in its neighborhood and outside of the boundary-layer.
- It delays separation and interferes with the evolution of the wake.

Detailed historical progress and developments in the field of Moving Surface Boundary-layer Control (MSBC) have been summarized by Modi (see Ref. [9]).

In the last decade, active flow control has assumed wider ramifications with a focus on optimal control strategies, as it directly translates into energy savings. A variety of control algorithms (both reactive and non-reactive type) have emerged in the non-linear dynamics and control community such as, chaos control [11], synchronization based control [12], pinning control [13], sporadic feedback control [14] etc. It is highly interesting to see how these control techniques (some of them being model control) can be integrated to exploit practically useful problems of engineering interest, such as fluid flow instabilities. In the context of flow past a circular cylinder, vortex shedding due to von Kármán is the first global instability mode, which needs to be predicted and controlled before attempting the control of higher modes that involve turbulence. The latter also arises in the range of moderate to high Reynolds numbers. Several promising strategies such as pinning control have been applied in the literature [13]. The idea of pinning can also be viewed in the context of synchronization, where the objective is to synchronize a chaotic system with the help of a target system [12,15]. In our earlier investigations [16], we have successfully established a closed loop feedback control strategy to suppress vortex shedding behind a D-shaped cylinder. This computational model control was experimentally implemented by Beaudoin et al. [17,18] and they have demonstrated effective control over the recirculation zones. Often, in the literature, the popular Ginzburg-Landau (G-L) equation is used to model the cylinder wake as it is straightforward to numerically integrate the amplitude equation, which enables rapid prototyping of control strategies [19,20].

A variety of passive flow control techniques are often used for the suppression of vortex induced oscillations such as, splitter plates, axial slats, fairings, helical strakes etc [5]. As opposed to passive techniques, active flow control requires additional power input and can be applied without any modifications to the geometrical configuration. On the cylinder surface, blowing and suction is used as a means of control in Refs. [21,22], for the purpose of wake stabilization. A systematic control method was developed by Min and Choi [23] using a suboptimal feedback control scheme. Oscillatory motion of the cylinder [24,25] and external forcing through acoustic excitation [26,27] are also popular in the literature. The latter has the potential to provide an intelligent control methodology, as evidenced in the suppression of open cavity flow oscillations related to aerospace problems [28]. With the advent of MEMS based technologies and development of smart materials, which involves intelligent sensing and actuator techniques, methods such as electromagnetic forcing [29,30] and piezo-electric actuation [31] are becoming popular. In a combustion application [32] electromagnetic flap actuators are used to manipulate the flame characteristics. Lifted flames could be controlled to achieve combustion stability and reduced toxic emission. Gerhard et al. [33] have presented a low-dimensional Galerkin model for the suppression of vortex shedding behind a circular cylinder. These lower order models are typically constructed from Karhunen-Loève decomposition in the from of POD tools. Lumley and Blossey [34] have laid out a broad framework for the control of turbulence, which can be generalized for the purpose of understanding generic flow control mechanisms. The essential ingredients of this algorithm include a large number of sensors (that report the state of the flow), a number of actuators (to enable actions to be performed and in what proportion and at what instant) and a control algorithm (to decide and parametrize the extent of these interactions).

In the present study, along with the mass and momentum conservation equations, a control equation is designed and implemented to achieve desired flow control goals. A large number of sensors are chosen downstream of the body to report the state of the flow. The role of externally controllable actuators on the fluid flow patterns past a circular configuration is assessed. The generic framework for wake control is pictorially depicted in Fig. 1. Here, the multiple-feedback sensors report the dynamic state of the flow and an algorithm would synthesize the quantum of actuations (with zero-net mass injection) to be performed. Such flow manipulations are achieved by means of locating two rotating

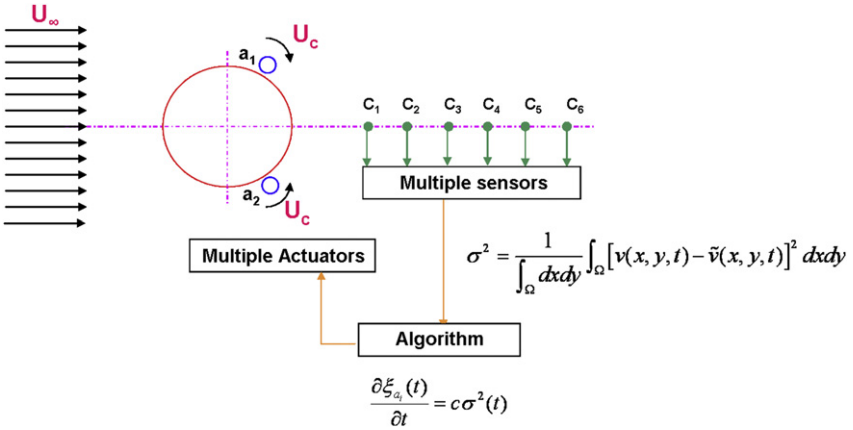

Fig. 1. Generic framework for the closed-loop feedback control, involving actuators (a_1, a_2, a_3,…), multiple-sensors (c_1, c_2, c_3…) and the control algorithm. The governing equations related to the control algorithm, and the multiple sensors are also indicated in the schematic. Here, the objective is to synchronize the current state of the system ($v(x, y, t)$) towards the desired target state ($\tilde{v}(x, y, t)$).

Please cite this article in press as: S. Muddada, B.S.V. Patnaik, An active flow control strategy for the suppression of vortex structures behind a circular cylinder, European Journal of Mechanics B/Fluids (2009), doi:10.1016/j.euromechflu.2009.11.002

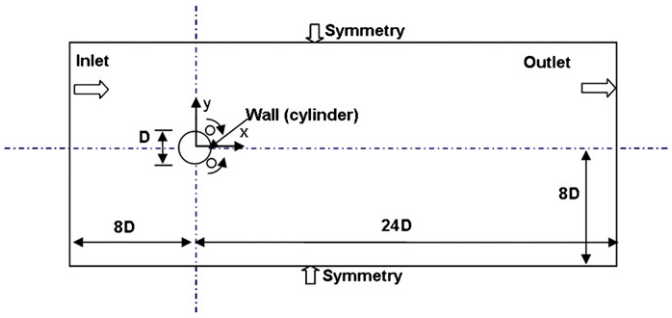

Fig. 2. Computational domain of interest with boundary conditions.

elements right behind the main cylinder. Practical realization of such control elements can be easily implemented by using hollow and bearing mounted configurations that can be either rotated clock-wise or counter-clock-wise. Similar feedback control was implemented in our earlier investigations on a D-cylinder [16]. However, any motor-driven rotating cylinder which is employed as an actuator will require energy expenditure. This issue is recently addressed by Beaudoin et al. [17,18] by constructing an objective function to quantify the associated costs. In their investigations, the net reduction in drag is assessed vis-á-vis the associated energy penalty for the actuators. In all these investigations, the actuators (in the form of control cylinders) are part and parcel of the bluff body itself. However, it should be noted that, in wind and structural engineering practice, it is not always plausible to have the actuators as an integral part of the main configuration. Furthermore, an engineering solution to existing vortex induced structural oscillations is possible without making any changes to the original configuration by keeping the actuators right behind the main cylinder. To this end, we choose two control cylinders in the vicinity of the main cylinder which are located in the wake region to investigate the influence of rotations on the wake region and the vortex street. With the above background, the present study focuses on the following objectives.

- To design and implement a simple proportional feedback reactive control strategy for the rotation parameter $\xi = U_c(t)/U_\infty$, which uses input from multiple-sensors and determines the actuator response.
- Numerically simulate and validate the flow past a circular cylinder. To control the vortex structures by means of actuators with the help of sensors and a control technique.
- To assess the influence of rotation parameter on the fluid flow features of interest such as streamlines, streaklines, vorticity contours etc and validate them with experimental fluid flow patterns.
- To quantify the vortex shedding frequency (the Strouhal number) and the associated fluid dynamic forces such as lift and drag.
- To be able to fine tune the nature of flow control, switching the actuators into either *on* or *off* state is performed to quantify the fluid dynamic forces and the associated suppression of vortex structures.
- To model the cost functional and analyze the optimal rotation in the context of drag reduction vis-á-vis the energy expenditure in imparting rotations to the actuators.
- To investigate the lag response to nimble periodic control and the resulting fluid flow forces on the body with the objective of further reducing the total energy expenditure.

2. Numerical scheme and solution methodology

2.1. Governing equations and numerical methodology

In the present study, the fluid flow features are modeled by assuming a two dimensional, unsteady, viscous and incompressible flow with constant fluid properties past a cylindrical configuration with two control cylinders. The governing equations for mass and momentum conservation, in non-dimensional form, are expressed as follows:

$$\frac{\partial u}{\partial x} + \frac{\partial v}{\partial y} = 0; \tag{1}$$

$$\frac{\partial u}{\partial \tau} + u\frac{\partial u}{\partial x} + v\frac{\partial u}{\partial y} = -\frac{\partial p}{\partial x} + \frac{1}{\mathrm{Re}}\left(\frac{\partial^2 u}{\partial x^2} + \frac{\partial^2 u}{\partial y^2}\right) \tag{2}$$

$$\frac{\partial v}{\partial \tau} + u\frac{\partial v}{\partial x} + v\frac{\partial v}{\partial y} = -\frac{\partial p}{\partial y} + \frac{1}{\mathrm{Re}}\left(\frac{\partial^2 v}{\partial x^2} + \frac{\partial^2 v}{\partial y^2}\right) \tag{3}$$

All geometrical lengths are normalized with the size of cylinder diameter (D), stream wise and cross-stream velocities with the inlet velocity (U_∞), physical time (τ) with (D/U_∞), and pressure (p) with (ρU_∞^2), where ρ refers to the fluid density.

Choosing the numerical flow domain, which is *just right* (neither too big nor too small), is still an art in computational fluid

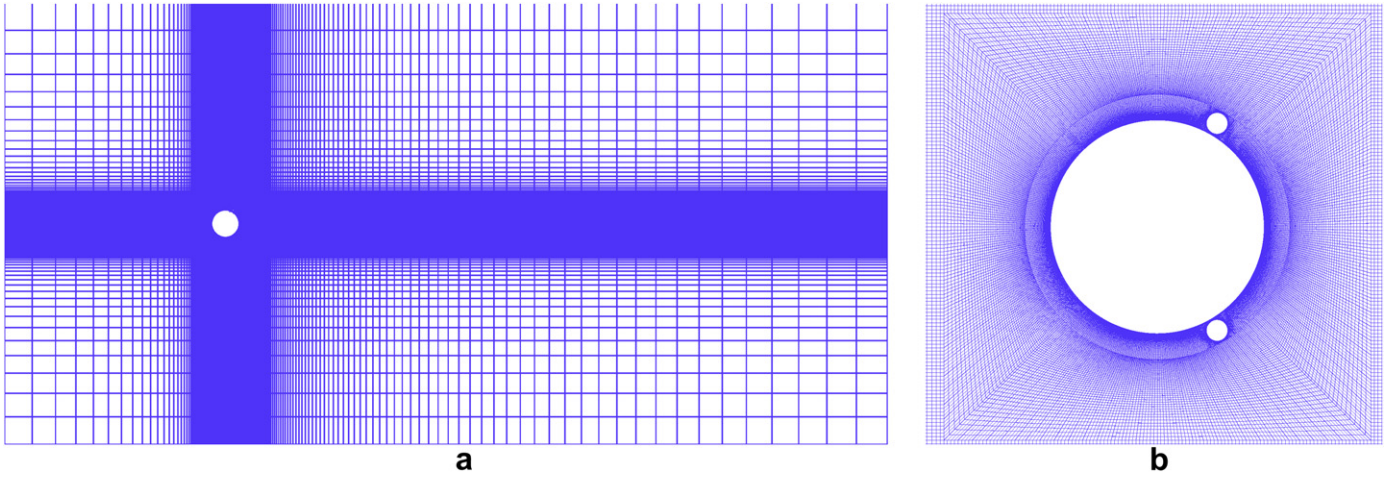

Fig. 3. (a). Discretization of the computational domain and (b). a close-up view of the grid resolution in the vicinity of the main cylinder.

Please cite this article in press as: S. Muddada, B.S.V. Patnaik, An active flow control strategy for the suppression of vortex structures behind a circular cylinder, European Journal of Mechanics B/Fluids (2009), doi:10.1016/j.euromechflu.2009.11.002

Fig. 4. Validation for (a) numerically resolved streaklines for $Re = 100$ (b) experimental visual of Taneda [38] for $Re = 140$. Note in particular, the remarkable similarity in the eddy shedding process and the connection between all the shed eddies through an *umbilical chord*.

dynamics. The free stream boundary conditions should theoretically be located at infinity. However, in reality, only a finite computational domain can be chosen in the numerical simulations. Hence, it is important to locate the in-flow, far-field and out-flow boundaries sufficiently far away from the cylindrical system under investigation so that the boundary conditions do not introduce any significant undesirable effects. The flow domain of interest with corresponding boundary conditions is shown in Fig. 2. The in-flow boundary is located at 8 times the diameter of the circular cylinder towards its fore, while the exit boundary is placed 24 times the cylinder diameter towards the aft. The free stream velocity is imposed on the in-flow boundary. No-slip is enforced on the circular cylinder and rotating elements. The boundary conditions $\partial u/\partial x = 0$, $\partial v/\partial x = 0$ are applied on the exit boundary. For the far field, symmetry boundary conditions ($\partial u/\partial y = 0$, $v = 0$) are applied. The computational domain of interest is tessellated with a non-homogeneous grid as shown in Fig. 3(a). A close-up view of the mesh is also provided in Fig. 3(b). In particular, a fine mesh is employed in all the zones where the gradients are likely to be very high, such as no-slip surfaces and the wake region.

The popular finite volume based SIMPLE scheme [35], which is incorporated in FLUENT [36] is used in our numerical calculations. The second order accurate semi-implicit scheme is chosen for the time integration. The spatial discretization is performed on a standard collocated grid using finite volume method. The detailed method of solution is available in many published works [35,37].

Briefly, in the Semi-Implicit Pressure Linked Equation (SIMPLE) solver, the pressure gradient is treated implicitly at $(n+1)$'th, time level, while all other terms are explicitly treated at (n)'th time level. The practical implementation of the scheme is achieved through the computation of intermediate velocities (*), which do not satisfy mass conservation. Subsequently, in the velocity correction phase, these values are projected into the divergence free vector space and corrected.

However, ahead of the velocity correction phase, the following, Poisson equation needs to be solved,

$$\nabla^2\left(p^{n+1} - p^*\right) = -\frac{1}{\Delta t}\left(\frac{\partial u^*}{\partial x} + \frac{\partial v^*}{\partial y}\right) \tag{4}$$

The details related to the flow solver and spatial discretization are discussed in detail in References [35,37].

2.2. Active flow control algorithm

The algorithm is depicted in the form a schematic in Fig. 1, where the recipe includes multiple-sensors, actuators and an algorithm that handles both sensors and actuators. Gillies [20] suggested multiple sensor feedback control to be more effective than single-sensor feedback control to achieve vortex shedding suppression. In Fig. 1, the sensors are identified by c_1, c_2, c_3 etc, while the actuators are indicated by a_1, a_2, a_3 etc. The sensors monitor the state of both stream-wise and cross-stream velocity values as a function of time. The total variance $\sigma^2(t)$ as a function of time is constructed and the control equation specified in (6) is employed to decide the quantum of actuations. Here, the objective is to implement a synchronization based coupling strategy between the current state of the flow ($v(x, y, t)$) and the desired target state ($\tilde{v}(x, y, t)$) and is implemented through Eqs. (5),(6). Here, the synchronization is taken to mean complete suppression of fluid flow oscillations. Therefore, the target state is a quiescent state given by $\tilde{v}(x, y, t)$ along the wake centerline. Total variance that varies as a function of time is given by,

$$\sigma^2(t) = \frac{1}{\int_{\Omega} \mathrm{d}x\mathrm{d}y} \int_{\Omega} \left[v(x, y, t) - \tilde{v}(x, y, t)\right]^2 \mathrm{d}x\mathrm{d}y \tag{5}$$

where Ω denotes the region behind the circular cylinder. However, the above integration boils down to a summation in the discrete version, as the sensors are placed only along the line of symmetry. The total variance in turn decides the extent of actuations to be employed through the rotating elements. The rotation parameter (ξ) is the ratio of control cylinder velocity to the free stream velocity, $\xi = U_c(t)/U_\infty$ is given by the equation below:

$$\frac{\mathrm{d}\xi(t)_{a_i}}{\mathrm{d}t} = C\sigma^2(t) \tag{6}$$

The control Eq. (6) described above is a generic one that injects momentum and it is implemented as a user defined function (UDF) and solved simultaneously with the Navier–Stokes equations. Here, the coefficient C is a proportionality constant and can be varied like a fuzz factor. This set of coupled equations render an opportunity to monitor the gradual control of wake instabilities. Momentum injection is initiated when the control cylinders start rotating which is actuated by applying power input. This generic flow control strategy of feedback sensors and actuators can indeed be

Table 1
Comparison of average drag, RMS lift coefficients and Strouhal number values for flow past an isolated circular cylinder for $Re = 100$. SUP: second order upwind, Q: QUICK scheme.

S.No	Reference	$\overline{C}_d$	St	$C_{l,rms}$
1	Engelman and Jamina [40]	1.40	0.170	0.257
2	Kang et al. [41]	1.34	0.164	0.236
3	Beher et al. [42]	1.41	0.170	–
4	Sharman et al. [43]	1.32	0.164	0.230
5	Jordan and Fromm [44]	1.28	0.16	–
6	Burbeau et al. [45]	1.41	0.164	0.257
7	Posdziech and Grundmann [46]	1.35	0.167	–
8	Present study (SUP)	1.39	0.170	0.237
9	Present study (Q)	1.40	0.170	0.240

Please cite this article in press as: S. Muddada, B.S.V. Patnaik, An active flow control strategy for the suppression of vortex structures behind a circular cylinder, European Journal of Mechanics B/Fluids (2009), doi:10.1016/j.euromechflu.2009.11.002

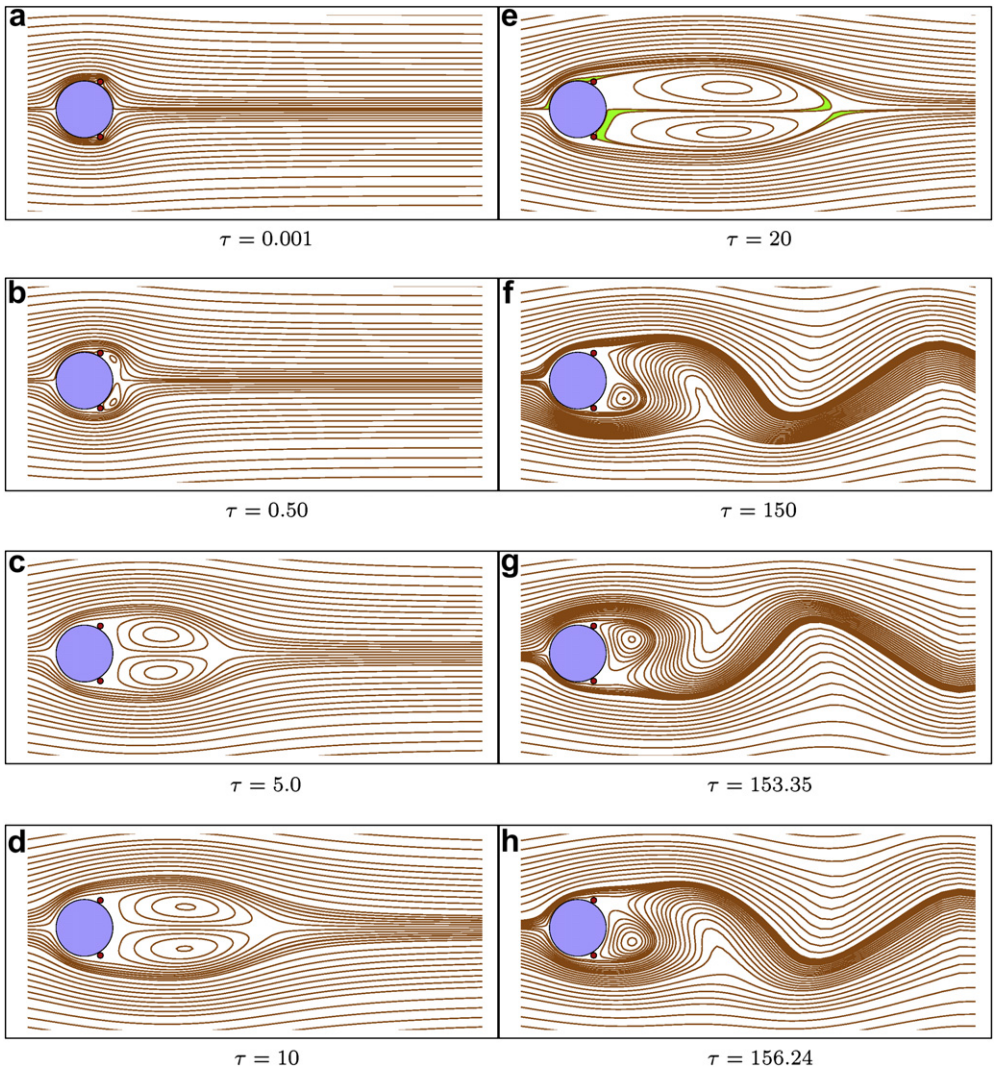

Fig. 5. Temporal evolution of streamline patterns for flow over a circular cylinder with control cylinders ($\xi = 0$) at $Re = 100$. The flow separation, twin eddy formation, inception of vortex shedding and periodic vortex formation can be noticed.

applied irrespective of the type of flow (both laminar and turbulent). In the present study, we investigate only sub-critical Reynolds number regime as it is a necessary precursor to any complicated investigations involving turbulence control.

3. Results and discussion

In this section we describe the closed loop flow control strategy employed in the present algorithm, for the simulation, annihilation and nimble control associated with the vortex structures. Extensive validation for flow past a circular cylinder is presented in Section 3.1. In Section 3.2 the influence of actuators (imparted through control cylinder rotations) on the vortex structures and the wake region behind the cylinder is discussed. The forces on the main cylindrical configuration and other design parameters of interest are also presented. In Section 3.3 the control equation is integrated along with the mass, momentum conservation equations and the extent of actuator input is evolved through the implementation of the flow control algorithm. To this end, the expenditure due to energy input is assessed in Section 3.5 and the robustness of the algorithm to perform sensitive (nimble) control operations is verified in Section 3.4.

3.1. Flow past an isolated circular cylinder

Simulation of complex fluid flow patterns behind bluff bodies is a challenging task. Capturing the main features of the flow field and associated fluid dynamical parameters of design interest is the primary objective of any Computational Fluid Dynamics (CFD) study. Before proceeding to the problem under investigation, the first logical step would be to demonstrate the usefulness of the procedure through its application to a well established problem. To that end, the classical problem of flow past an isolated circular cylinder in a sub-critical range of Reynolds numbers is considered for validation. Streakline visuals depicted in Fig. 4 are validated against the experiments of Taneda (see [38]). The distinct feature here is the gradual roll-up of shear layers at crests and troughs. It

Table 2
Mesh sensitivity study for flow past a circular cylinder with two control cylinders($\xi = 0$) at $Re = 100$.

S.No	Number of nodes	Number of cells	$\overline{C}_d$	St	$C_{l,rms}$
I	26 271	25 853	1.4791	0.172	0.294
II	53 154	52 584	1.4822	0.172	0.292
III	88 109	87 362	1.4787	0.172	0.286

Please cite this article in press as: S. Muddada, B.S.V. Patnaik, An active flow control strategy for the suppression of vortex structures behind a circular cylinder, European Journal of Mechanics B/Fluids (2009), doi:10.1016/j.euromechflu.2009.11.002

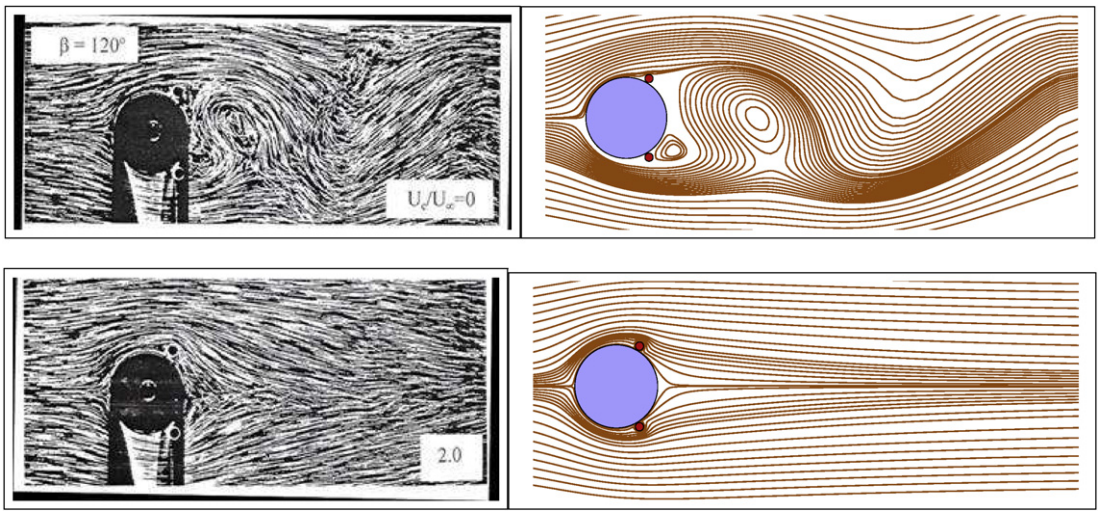

Fig. 6. Validation of numerical visualization for $Re = 100$, against experimental result [47]. Here, the two control cylinders are located at $\beta = 120^{\circ}$ to the flow direction. The rotation parameter $\xi = U_c/U_\infty$ represents rate of momentum injection into the wake region.

should be noted that all these eddies are mutually connected by a trail streakline which originates in the near wake. The experimental visual is produced by the illumination of a sheet of light, through electrolytic precipitation of a white colloidal smoke. Time averaged drag coefficient and Strouhal number values are compared with some of the earlier investigators (see Table 1), which are found to be in good agreement. Among the two schemes QUICK and streamline second order upwinding, the former is preferred owing to better agreement with other investigations. Coefficient of drag and Strouhal number are defined as follows:

$$\overline{C}_d = \frac{\overline{F}_D}{\frac{1}{2}\rho U_\infty^2}; St = \frac{f_{vs} D}{U_\infty} \tag{7}$$

where $\overline{F}_D$ is the mean drag force per unit area and f_{vs} is the vortex shedding frequency. It should be pointed out that among these validations, achieving a good comparision of fluctuating lift force is relatively difficult. We have also performed a systematic mesh sensitivity study to eliminate the possibility of cell size dependence on the force coefficients and flow patterns.

3.2. Flow past a cylinder with two control cylinders

In this section, the flow past the main cylinder with two small rotating elements is presented. The two actuators in the form of control cylinders are located right behind the main cylinder (making an angle of 120° to the upstream vector). This angle has relevance as it is akin to tangentially enabling suction from the favorable pressure gradient region of the main cylinder and injection into the adverse pressure gradient side. Furthermore, it pushes high momentum shear layers closer to the no-slip surface of the main cylinder, as the adverse pressure gradient region starts around 90°. The top control cylinder is rotated clock-wise, while the bottom one is rotated counter-clockwise (see Fig. 2), to enable momentum injection into the wake region. The size of the main cylinder, rotating elements and the gap ratio are 1.0D: 0.1D: 0.01D respectively, where D refers to the diameter of the main cylinder. To start with, the temporal evolution of the flow past a cylinder with two control cylinders is simulated for $\xi = U_c/U_\infty = 0.0$ in Section 3.2.1. The role played by the actuators through the control algorithm is discussed in Section 3.3.

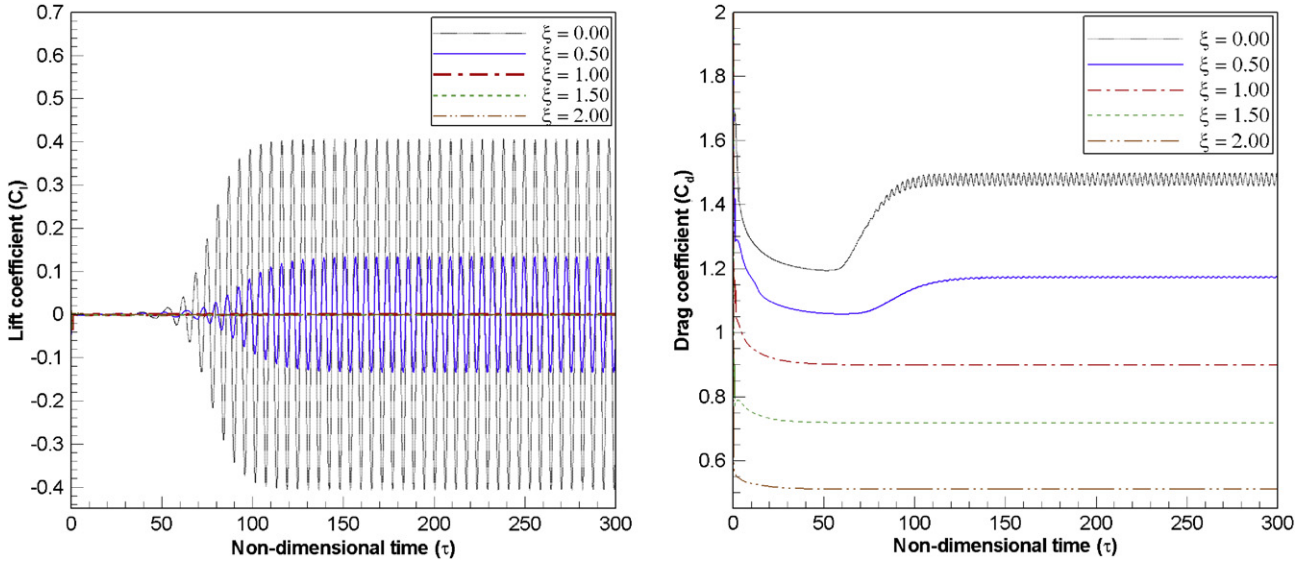

Fig. 7. Comparison of lift and drag coefficient histories for different rotation parameter (ξ) values for $Re = 100$.

Please cite this article in press as: S. Muddada, B.S.V. Patnaik, An active flow control strategy for the suppression of vortex structures behind a circular cylinder, European Journal of Mechanics B/Fluids (2009), doi:10.1016/j.euromechflu.2009.11.002

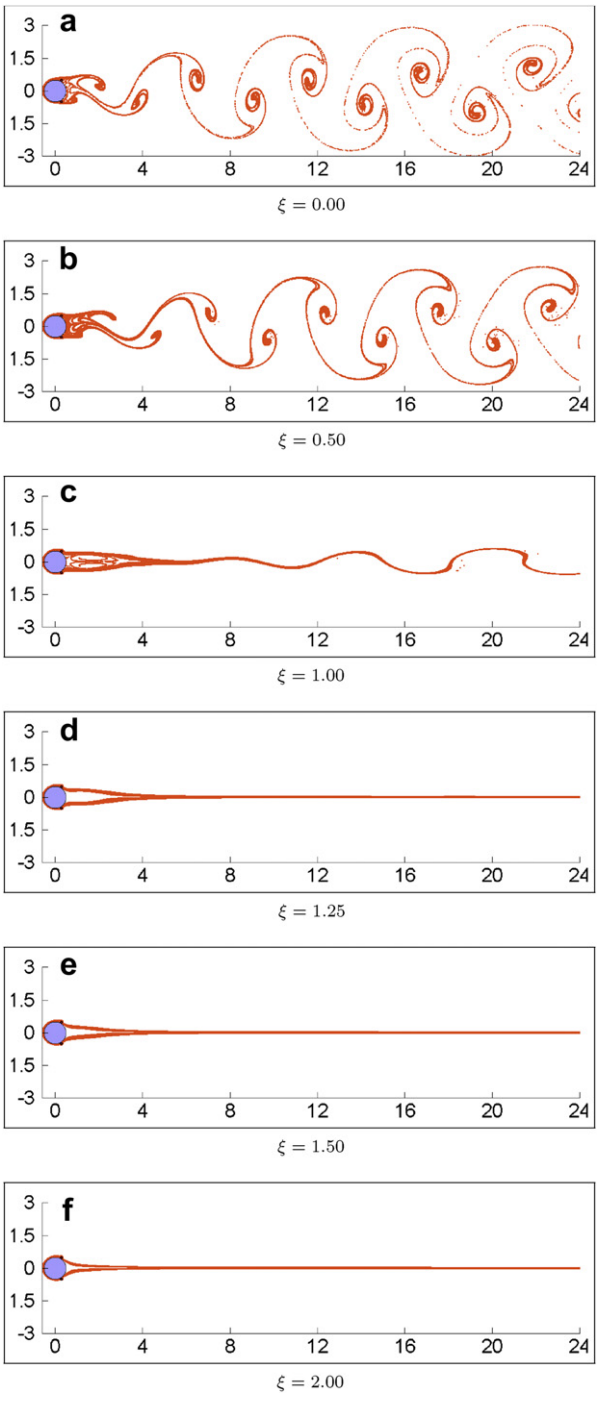

Fig. 8. Streakline patterns for different rotation parameters at $Re = 100$.

3.2.1. The impulsive start

To start with, the computational algorithm is used to describe the near wake at early instants of time, which is also known in the literature as the *impulsive start*. Streamlines depict the instantaneous snapshot of the fluid flow behavior at a particular instant of time. Compared to velocity vectors, they provide a better visual appreciation of the fluid flow characteristics. The influence of rate of rotation ($\xi = U_c/U_\infty$) on the wake is assessed through the investigations at specific values of ξ. The case of two control cylinders kept stationary with $\xi = U_c/U_\infty = 0.0$ is investigated. The temporal evolution, for the case where both control cylinders are not rotating, is shown in Fig. 5. In the beginning ($\tau = 0.001$), the

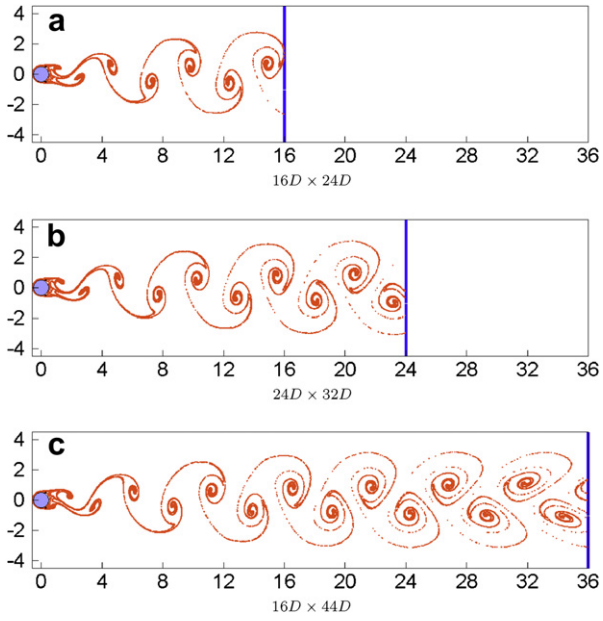

Fig. 9. The influence of exit boundary (shown as a blue line online) on the vortex formation and streakline generation for $Re = 100$; $\xi = 0.0$. The lack of reflection due to the presence of exit boundary on vortex formation can be particularly noticed.

flow has a fore and aft symmetry (Fig. 5a). With the percolation of viscous influences, the asymmetry on the aft, sets in as shown in Fig. 5(b). The formation of two symmetric attached eddies (popularly known as Föpal vortices), of opposite vorticity, can be noticed in Fig. 5(c). These eddies are fed by circulation from the shear layers, they grow in size ($\tau = 20$), and gradually become asymmetric. In particular note the presence of a passage way with a fascinating transfer of momentum; in this case from the outer edge of the top vortex, via central region, engulfing the lower edge of the bottom vortex (Fig. 5e). The figure in particular, identifies two streamlines undergoing crossover. Similar to that found in Fig. 5(e), using a thorough analysis of streamlines, Perry et al. [39] have shown that an *alley-way* passage is the precursor for the inception of vortex shedding. With further progress in time, vortex shedding begins

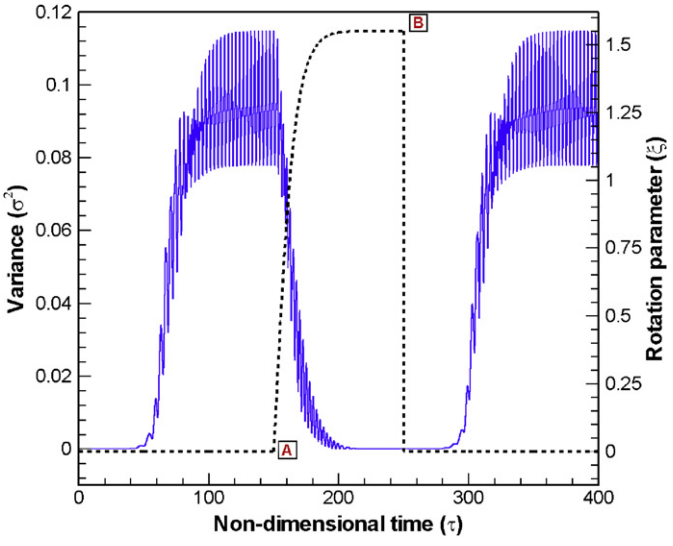

Fig. 10. Temporal evolution of total variance (solid line) and its associated rotation parameter (dashed line) for proportionality constant (C) = 1.0 at $Re = 100$. Point A refers to control being switched *on* and point B refers to control *off*.

Please cite this article in press as: S. Muddada, B.S.V. Patnaik, An active flow control strategy for the suppression of vortex structures behind a circular cylinder, European Journal of Mechanics B/Fluids (2009), doi:10.1016/j.euromechflu.2009.11.002

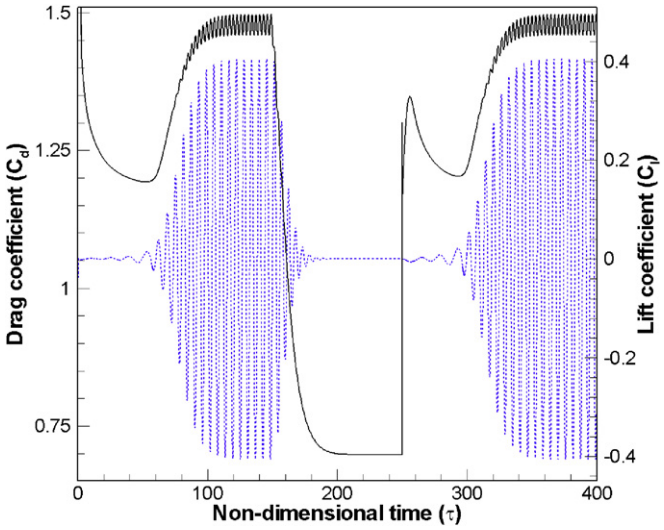

Fig. 11. Temporal history of lift coefficient (dashed line) and drag coefficient (solid line) for $C = 1.0$ in Eq. (6) at $Re = 100$.

and the wake becomes gradually tighter and more organized (Fig. 5(f)), which in turn induces periodic lift forces on the body. This periodic vortex shedding is also visible in the lift coefficient history. (Fig. 5(g–h)) indicate the sinusoidal nature of the flow patterns in the wake region and the presence of an eddy (either at the top or bottom) in the formation region.

For the case of a main cylinder with two control cylinders, systematic grid sensitivity studies are also carried out. At least, three types of grid sizes have been employed to check for the grid dependence (see Table 2). The fluid flow forces on the main cylinder (in the form of lift and drag forces) and the Strouhal number are compared. Since, these design parameters have less than 1–2% change, between type II and III mesh sizes, the latter mesh is found to be suitable for subsequent calculations.

3.2.2. *Influence of actuators on the main cylinder*

In this section we investigate the influence of actuators (control cylinder rotation) on the vortex structures behind the main cylinder. Fig. 6 depicts the influence of a fixed rotation parameter on the numerically simulated flow patterns. In the absence of control cylinder rotation ($U_c/U_\infty = 0$), vortex formation behind the cylinder is effectively captured. However, when rotations are triggered, momentum is injected into the wake region and for small values of rotation parameters, the vortex formation is gradually disrupted. For $U_c/U_\infty = 2.0$, the separated streamlines converge to form a *V-cone* like formation in the aft region, thus approaching the *potential* flow character. To get a better physical appreciation of the complex nature of the flow field, a flow visualization study was under taken. The flow visualization was conducted in a closed circuit water channel facility. The model was constructed using

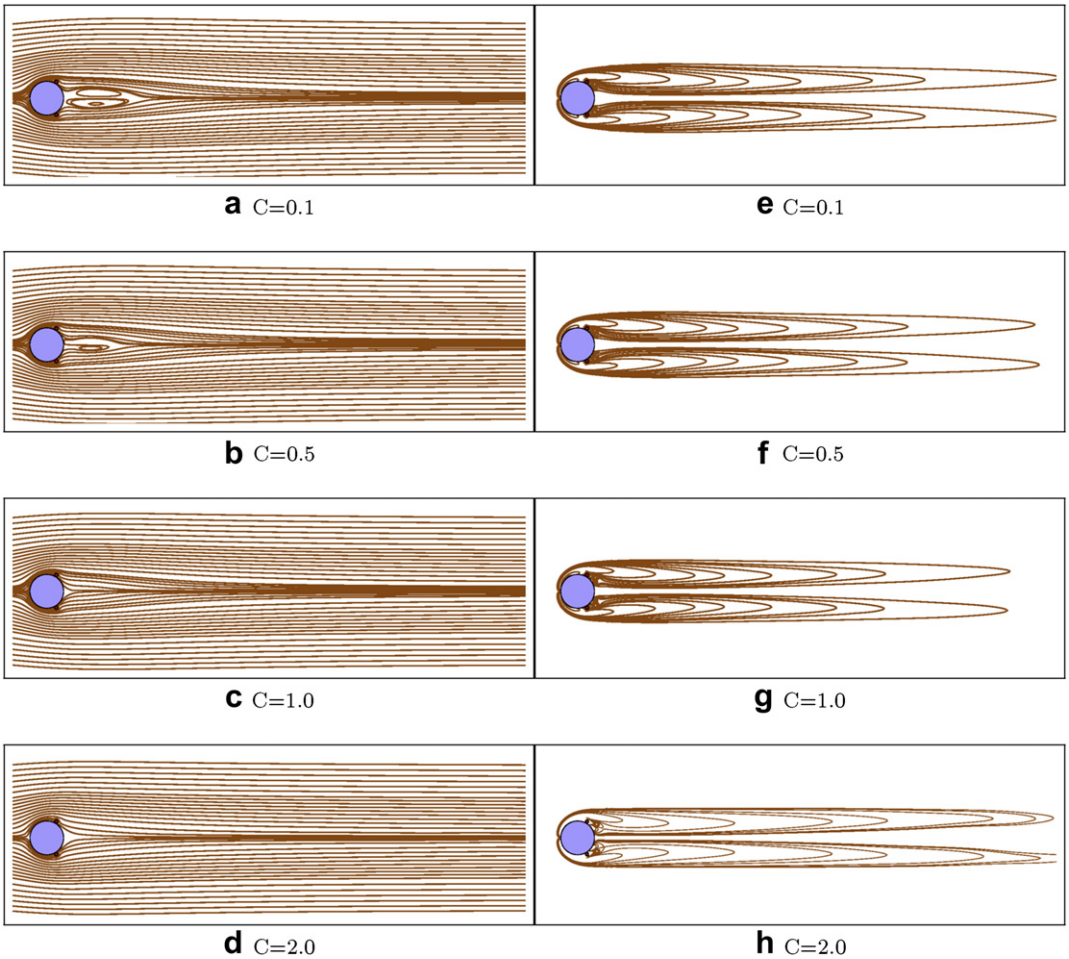

Fig. 12. Influence of proportionality coefficient C on streamlines (a–d) and vorticity contours (e–h) for $Re = 100$. Note in particular, the wake region has a persistent weak twin eddy pattern for lower values of C.

Please cite this article in press as: S. Muddada, B.S.V. Patnaik, An active flow control strategy for the suppression of vortex structures behind a circular cylinder, European Journal of Mechanics B/Fluids (2009), doi:10.1016/j.euromechflu.2009.11.002

Table 3
Dependence of proportionality coefficient (C) in Eq. (6) for $Re = 100$; on maximum steady state rotation parameter ξ_{max} and the corresponding mean drag coefficient ($\overline{C}_d$). ΔT_s refers to the non-dimensional time required to reach steady state.

S.No	C	ξ_{max}	ΔT_s	$\overline{C}_d$
1	0.1	1.07	624	0.901
2	0.5	1.23	149	0.852
3	1.0	1.55	68	0.697
4	2.0	1.95	42	0.602

plexiglass and fitted with rotating cylinders driven by variable speed motors. Aluminum powder suspensions were used in conjunction with slit lighting to visualize the streamlines. The air–water interface thus captured with the aid of *Aluminum* dust as the passive tracer depicts the effectiveness of the momentum injection and the role of actuators in the reduction of wake width as in Fig. 6. The correlation between numerical predictions (Fig. 6) and flow visualization results is indeed satisfactory considering the complex character of the flow. In the absence of any rotations ($U_c/U_\infty = 0.0$), the two actuators remain immersed in the separated flow field. This results in a wider wake, and the downstream is dominated by eddy formation and shedding. The figure depicts a large vortex, which is about to get washed away into the wake. As noted by Perry et al. [39], a saddle point type of instability associated with the newly formed vortex is discernible. The overall configuration of the wake reverses itself in an alternating fashion in compliance with the vortex shedding process. The shed vortices grow rapidly as they are convected downstream, diffusing vorticity in the surrounding region at a faster rate. When the control cylinders are cranked with even higher rotation rates, say $\xi = 2.0$, the wake gradually becomes narrower and the vortex formation is completely suppressed. For this rotation parameter, the boundary-layer remains totally attached to the main cylinder and vortex shedding ceases completely. The flow domain becomes completely *inviscid like* in its appearance. In the near wake of the cylinder, a *V-cone* type formation is seen both in the experimental and numerical visuals.

The lift and drag forces are obtained by integrating the normal and tangential stresses due to pressure and velocity gradients as given below:

$$C_d = 2\oint\left\{-p\mathrm{d}y + \frac{1}{\mathrm{Re}}\left[2\frac{\partial u}{\partial x}\mathrm{d}y + \left[\frac{\partial u}{\partial y} + \frac{\partial v}{\partial x}\right]\mathrm{d}x\right]\right\} \tag{8}$$

$$C_l = 2\oint\left\{-p\mathrm{d}x + \frac{1}{\mathrm{Re}}\left[2\frac{\partial u}{\partial x}\mathrm{d}x + \left[\frac{\partial u}{\partial y} + \frac{\partial v}{\partial x}\right]\mathrm{d}y\right]\right\} \tag{9}$$

The schematic Fig. 7(a),(b) represents the temporal histories of the fluid flow forces on the main cylinder. The actual design parameters of interest such as RMS lift and mean drag coefficient can be deduced from these lift and drag coefficient histories respectively.

3.2.3. Streakline visualization

The streamlines are essentially flow lines, which reflect the instantaneous nature of the flow. Pressure, vorticity contours *etc* are also instantaneous snap-shots of the flow. However, their capability to truly project the unsteady nature of the spatio-temporal history of the wake is quite limited. Experimental flow visualization techniques typically employ a physical tracer source such as hydrogen bubbles, tufts, oil films, smoke particles, dye, Aluminum dust etc. The present investigation closely emulates this procedure and uses the release of pseudo particles. The problem of tracer getting diffused with the main flow is highly likely in an experimental visualization. However, the numerical approach is devoid of any such interaction with the primary flow, which is an added advantage. Streakline visuals are obtained by the release of about 50–60 particles from distinct and suitably chosen locations on the fore side of the main cylinder. These particles are released at regular intervals (which is different from the integration time-step Δt), until they reflect a qualitative streakline picture reflecting the wake patterns. In the present investigation, a simple approach is devised to obtain the detailed structure of the wake through streaklines, which solves the following equation:

$$\frac{\mathrm{d}x_i}{\mathrm{d}t} = u_i \quad \forall i : 1\cdots P. \tag{10}$$

where, P refers to the total number of particles which are released from distinct sources on the fore of the cylinder. This equation is suitably integrated from their initial positions as the passive scalars move along with the flow field (without any inertial influences). The numerical streakline plot thus obtained by employing passive tracers is presented in Fig. 8. When the rotation parameter ($\xi = U_c/U_\infty$) is set to 0.0, it results in a wider wake than expected in the case of an isolated circular cylinder. This is primarily because of the twin control cylinders in the aft region, which together makes the configuration look like a single lobe shaped object. The particles thus released, imbibe the spatio-temporal history of the wake and capture the unsteady vortex shedding process rather vividly as depicted in Fig. 8(a,b). When the cylinders are set into rotation mode, with $\xi = 0.5$ (Fig. 8(b)), vortex shedding still persists, but the wake width is reduced. In connection with vortex shedding behind a circular cylinder, by means of a number of schematics, Perry et al. [39] have shown that, every shed eddy is ultimately inter connected to every other eddy by its own *umbilical chord* or *thread*. This aspect could be distinctly visualized in Fig. 8(a) to (b). Also, notice the eddy curl-up and the reduced residence time can be surmised for these two cases. When still higher rotation rates are imparted to the control cylinders, i.e. $\xi = 1.0$, the vortex shedding is suppressed with a persistent twin eddy pattern behind the main cylinder. Interestingly enough, this is the route through which the vortex shedding inception happened as discussed in Section 3.2.1. However, the instabilities present in the near wake zone are not strong enough to feed more circulation into the shear layers to enable vortex shedding. Interestingly, the convective instability in the far wake still persists. This can be confirmed from the sinusoidal nature of the streakline plot in Fig. 8(c). For still higher rotation rates, $\xi = 1.25$, 1.50 and 2.00, a narrow band of inviscid like streakline plot is seen in Fig. 8(d–f). Here, as expected, the particles

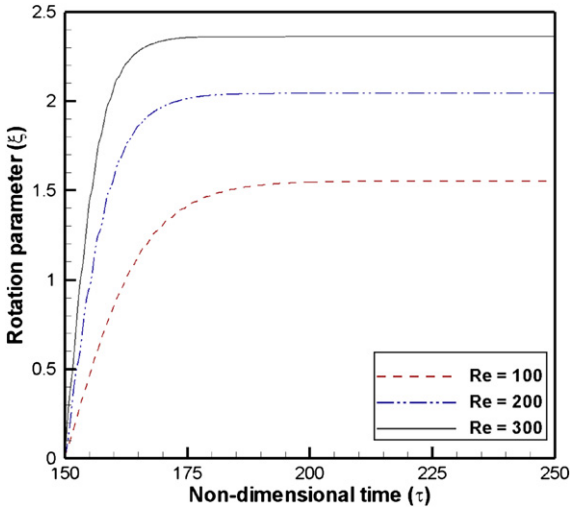

Fig. 13. Comparison of temporal evolution of rotation parameter for different Reynolds numbers ($C = 1.0$).

Please cite this article in press as: S. Muddada, B.S.V. Patnaik, An active flow control strategy for the suppression of vortex structures behind a circular cylinder, European Journal of Mechanics B/Fluids (2009), doi:10.1016/j.euromechflu.2009.11.002

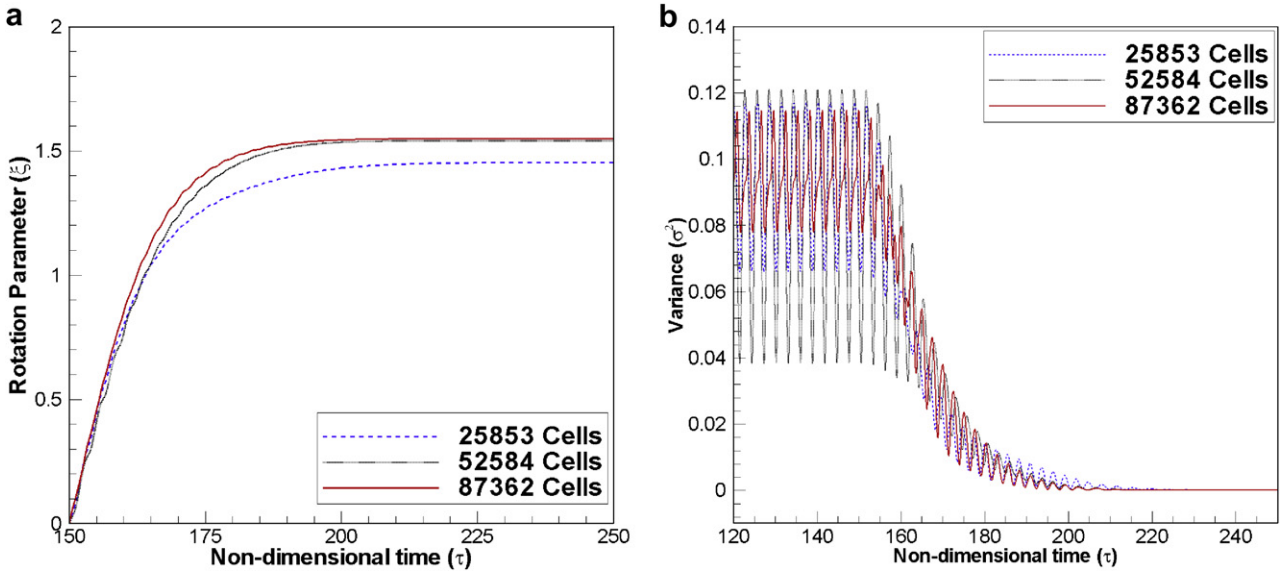

Fig. 14. Grid sensitivity study for $Re = 100$ ($C = 1.0$). (a) Influence on $\xi(t)$. (b) Influence on $\sigma^2(t)$.

released are unable to penetrate the small cavity region behind the cylinder, which are having small twin eddies. For these steady fluid flow cases, both streaklines and streamlines are now synonymous in their representation. The influence of in-flow, exit and far-field location effect was systematically studied by Posdziech and Grundmann [46] using a higly accurate spectral element. In the present investigation the exit boundary location is varied to study the influence on the vortex formation through streaklines as in Fig. 9. The traction free nature of the exit boundary, clearly suggests lack of any boundary effects such as those due to reflection.

3.3. Coupled, closed loop, automatic feedback reactive control

As explained in Section 2.2, the control algorithm actuates the control cylinders with an inherent time delay between sensing and actuation. However, under steady periodic conditions, such delays get evened out, and would lead to a synchronized target state. The variance term in the control equation is modified at every time step by updating the cross-stream component of velocity of the sensor signals in Eq. (5). The actuators are switched *on* (indicated by A), only after reaching steady periodic vortex shedding as shown in Fig. 10. The rate of injection of momentum (through $\xi(t)$) gradually picks up and reaches a steady state value, while the temporal variance ($\sigma^2(t)$) constructed out of the sensor points droops down. The concomitant changes in the fluctuating lift and drag forces are indicated in Fig. 11. There is a remarkable reduction of 53% in the mean drag value for $Re = 100$. In the context of a D-cylinder, similar drag reduction studies with the objective of achieving extremum seeking control have been performed by Beaudoin et al. [18]. They have reported a drag reduction of approximately 23% at injection ratios of order one. The controllers are switched *off* (as indicated by B), to verify the reactive nature of the controllers used in the present investigation. The variance and the fluctuating lift and drag forces can be seen to be back to their original range of full blown values, reflecting the periodic nature of the wake. As the fluid flow patterns evolve behind the circular cylinder, the instabilities lead to the onset of von Kármán vortex shedding. The proportionality coefficient used in Eq. (6), is indeed a kind of fuzz factor, which needs to be properly calibrated. To this end, the influence of three different coefficients ($C = 0.1$, 0.5, 1.0 and 2.0) are compared. It should be noticed that the higher the value of fuzz factor, the higher will be the rate of momentum injection and therefore, resulting in a higher value of steady state rotation parameter (ξ). Although $C = 0.1$ results in a smaller value of ξ, it takes much longer to reach such a steady state. Corresponding to the value of $C = 0.1$, 0.5, 1.0 and 2.0, streamlines and vorticity contours are presented in Fig. 12. For $C = 0.1$, the rate of rotation is not strong enough to penetrate the needle like alley-way which is located right behind the main cylinder. However, for $C = 1.0$, no such pattern (similar to the depleted twin eddy pattern) persists, which can be readily supported from Fig. 12. Therefore, it can be seen that $C = 1.0$ is a reasonable proportionality coefficient. It can be seen from Table 3, that it takes much longer to reach a steady state rotation parameter (ξ_{max}) for smaller C values. For $Re = 100$, 200 and 300, the corresponding rotation rates for steady state are 1.55, 2.04 and 2.36 respectively. The temporal evolution of $\xi(t)$ is plotted against time in Fig. 13. The grid resolution around the control cylinders would

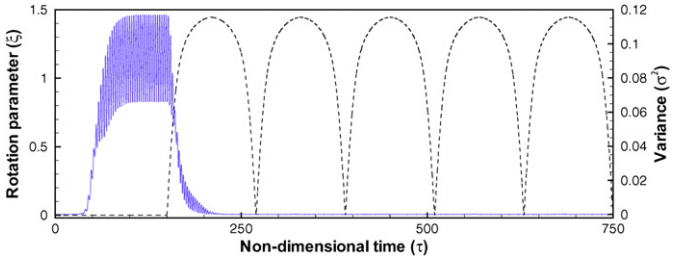

Fig. 15. Influence of repeated *on-off* control (nimble control) on variance (dotted line) and corresponding rotation parameter (dashed line) for $Re = 100$.

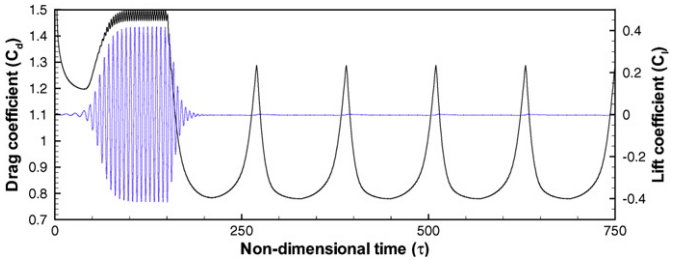

Fig. 16. Lift (dotted line) and Drag (solid line) coefficient variation under the influence of nimble control strategy for $Re = 100$.

Please cite this article in press as: S. Muddada, B.S.V. Patnaik, An active flow control strategy for the suppression of vortex structures behind a circular cylinder, European Journal of Mechanics B/Fluids (2009), doi:10.1016/j.euromechflu.2009.11.002

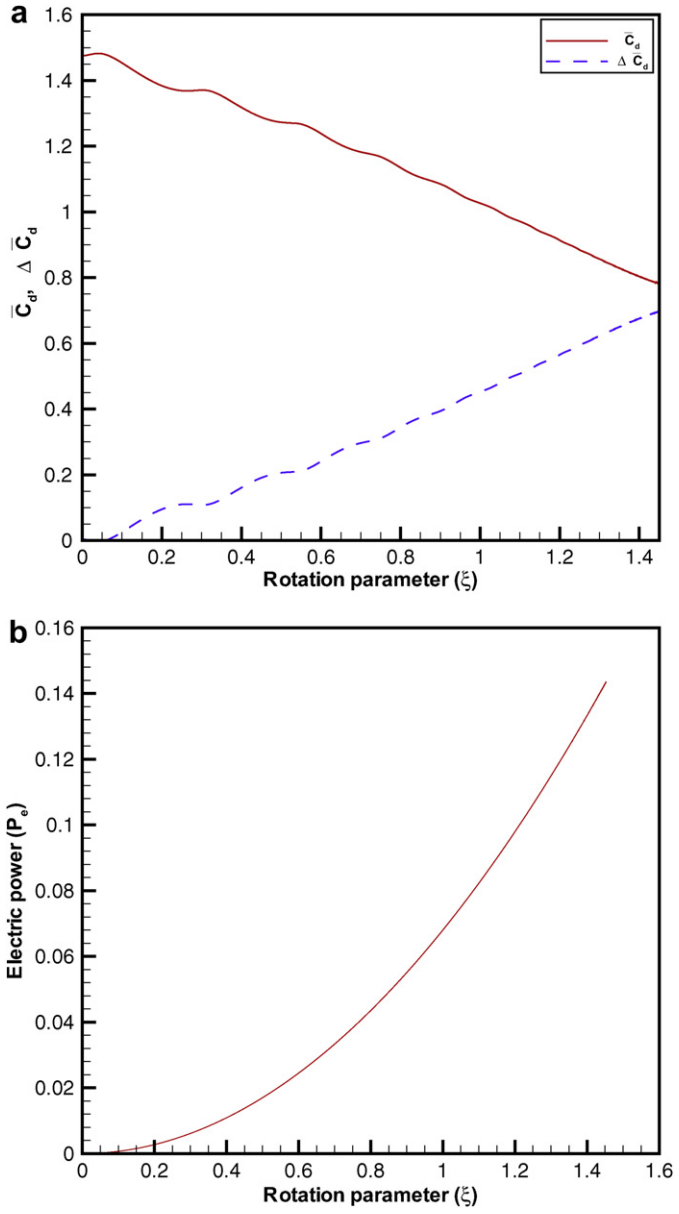

Fig. 17. (a) Variation of mean drag coefficient ($\overline{C}_d$) and net drag savings ($\Delta\overline{C}_d = \overline{C}_{d_{\xi=0}} - \overline{C}_{d_\xi}$) with rotation parameter and (b) Modeled electric power consumption with rotation parameter for $Re = 100$.

impact the perculation of momentum injection influences. Mesh sensitivity effect, on both $\xi(t)$ and $\sigma^2(t)$ are shown in Fig. 14.

3.4. Nimble control

To be able to assess the sensitive dependence of rotation parameter ξ on the vortex structures, and the fluctuating lift and drag forces, it is highly desirable to see if continuous momentum injection is mandatory. For a chosen value of the fuzz factor ($C = 1.0$), the actuators should respond with the rotation parameter ξ that temporally varies as determined by the control algorithm. After reaching a maximum value of $\xi_{\max}$ (at steady state), it is gradually traced back at the same rate at which the momentum injection was achieved. This is indeed replicated using a mirror symmetry, after the system reaches a synchronized steady state. This entire cycle is repeated for at least five such periods (as shown in Fig. 15), to investigate the nimble control capability of the present algorithm. Surprisingly, the variance hovers close to a quiescent target state value. This counter intuitive result, further opens up the possibilities for experimental verification and validation vis-á-vis the cost reduction. At the outset, it may appear that such a nimble control is fairly complicated, however, it must be pointed out that, given the current state of art in system based controls, it is routinely possible to program even a more sophisticated methodology. The corresponding lift and drag histories are shown in Fig. 16. Although the RMS lift force coefficient is almost zero, the associated drag coefficient is only 25% less than the mean drag coefficient as against the 53% achieved under maximum steady rotation parameter.

3.5. A model for cost function analysis

In the present context, the actuators are essentially simple control cylinders, which rotate and inject momentum into the boundary layer and the near wake region. Imparting rotations through a control algorithm requires energy expenditure. It is therefore imperative to ensure that the energy expenditure incurred is suitably subtracted from the energy savings, being accrued due to drag reduction. To this end, we perform a cost function analysis where the objective is to find out the value of optimum rotation parameter (ξ_{opt}). Furthermore, since it is shown that by employing the control algorithm, it is possible to obtain the suppression of vortex structures and the ensuing drag reduction. The coefficient of drag and the net drag reduction as a function of ξ are depicted in Fig. 17(a). Since it is well known that electric power consumption variation is a quadratic, given by the following equation

$$P_e = 2\alpha\xi^2(t) \tag{11}$$

Here, the proportionality coefficient (α), is typically obtained by modeling, through experimental measurements and by performing fitting and regression. The factor 2 in particular identifies the presence of two control cylinders in the present investigation. Following the experimental studies of Beaudoin et al. [17], and adopting a similar procedure we have chosen a value of $\alpha = 0.00085$. The corresponding electric power consumption is shown in Fig. 17(b). By noticing both net energy savings indicated by Fig. 17(a) and the modeled energy expenditure for actuations given by Fig. 17(b), we can obtain an optimum point where the total cost function will have a minimum. If the proportionality coefficient α is precise, it is possible to identify the corresponding ξ_{opt} that has the maximum energy savings.

4. Conclusions

In the present study, simulation of flow over a circular cylinder with multiple-feedback sensors and actuators is presented with the aid of a control algorithm. By designing a control equation, an automatic, closed loop reactive feedback strategy is implemented. Extensive validations are carried out on an isolated circular cylinder. Flow visuals in the form of streamlines, streaklines and vorticity contours depict effective wake control. The numerical calculations identify the influence of rotation parameter on the periodic vortex shedding, fluid flow features and the forces exerted by the fluid. Detailed parametric optimization with due quantification of cost penalty involved in momentum injection (with zero net mass) vis-á-vis experimental visualization is also presented.

Based on the results of the present investigation involving numerical calculations, and supportive flow visualization in the *Re* range of 100–300, the following conclusions can be made:

Please cite this article in press as: S. Muddada, B.S.V. Patnaik, An active flow control strategy for the suppression of vortex structures behind a circular cylinder, European Journal of Mechanics B/Fluids (2009), doi:10.1016/j.euromechflu.2009.11.002

- The vortex street is simulated and controlled by employing a simple reactive feedback control algorithm.
- Numerical and experimental flow visualization clearly demonstrated the effectiveness of the rotary type actuators (through zero-net mass injection) in modifying the vortex structure of the wake and hence vortex shedding, at two discrete levels of rotation, viz. $\xi = U_c/U_\infty = 0.0$, 2.0. For $U_c/U_\infty = 2.0$, it remains totally attached to the surface and the vortex shedding ceases completely. The flow is rather *inviscid like* in its appearance.
- The wake structure is revealed by tracking numerically released passive tracers. All the shed eddies are connected by an *umbilical chord*, for the case of zero rotation rate, i.e. for $U_c/U_\infty = 0.0$.
- It is found that the rate of steady state injection depends on the proportionality coefficient. Higher the rate of injection(also influenced by C), the faster it will reach steady state and vice-versa.
- The total cost function has an optimum (ξ_{opt}) depending on the energy savings through the momentum injection vis-á-vis the energy expenditure in enabling the actuators.
- For a steady state rotation parameter (ξ) = 1.55, for $Re = 100$, a remarkable 53% drag reduction could be achieved.
- It is demonstrated that energy expenditure can be further optimized through nimble control by enabling periodic switch *on* and *off* capability.

Acknowledgments

Authors would like to thank the two anonymous referees for their insightful comments. One of the authors (BSVP), thanks the center for IC & SR, IIT Madras, Chennai for funding computational facilities through grant no: APM/07-08/206/NFSC/BSVP. We thank Prof John Thuburn, University of Exeter, U.K. for his helpful comments on an earlier version of this paper.

References

[1] M.M. Zdravkovich, Flow Around Circular Cylinders, , In: Fundamentals, vol. 1. OUP, New York, 1997.
[2] C.H.K. Williamson, Vortex dynamics in the cylinder wake. Ann. Rev. Fluid Mech. 28 (1996) 477–539.
[3] K.R. Sreenivasan, Fluid turbulence. Rev. Mod. Phys. 71 (2) (1999) S383–S395.
[4] C.H.K. Williamson, R. Govardhan, Vortex-induced vibrations. Ann. Rev. Fluid Mech. 36 (2004) 413–455.
[5] R.D. Blevins, Flow Induced Vibrations. Von Nostrand Reinhold, 1990.
[6] B.S.V. Patnaik, P.A.A. Narayana, K.N. Seetharamu, Numerical simulation of laminar flow past a transversely vibrating circular cylinder. J. Sound Vib. 228 (3) (1999) 459–475.
[7] A. Roshko, Perspectives on bluff body aerodynamics. Int. J. Wind Eng. Ind. Aerodyn 49 (1993) 79–100.
[8] A. Betz, History of Boundary Layer Control in Germany. in: G.V. Lachmann (Ed.), Boundary Layer and Flow Control. Pergamon Press, New York, USA, 1961, pp. 1–20.
[9] V.J. Modi, Moving surface boundary-layer control: a review. J. Fluids Struct. 11 (1997) 627–663.
[10] F. Mokhtarian, V.J. Modi, Fluid dynamics of airfoils with moving surface boundary-layer control. J. Aircr. 25 (1988) 163–169.
[11] E. Ott, C. Grebogi, J.A. Yorke, Controlling chaos. Phys. Rev. Lett. 64 (11) (1990) 1196.
[12] G.W. Wei, Synchronization of single-side locally averaged adaptive coupling and its application to shock capturing. Phys. Rev. Lett. 86 (16) (2001) 3542–3545.
[13] G. Tang, S. Guan, G. Hu, Controlling flow turbulence with moving controllers. Eur. Phys. J. B 48 (2005) 259–264.
[14] G.N. Tang, G. Hu, Controlling flow turbulence using local pinning feedback. Chin. Phys. Lett. 23 (6) (2006) 1523–1526.
[15] S. Guan, G.W. Wei, C.H. Lai, Controllability of flow turbulence. Phys. Rev. E. 69 (2004) 066214.
[16] B.S.V. Patnaik, G.W. Wei, Controlling wake turbulence. Phys. Rev. Lett. 88 (2002) 054502.
[17] J.F. Beaudoin, O. Cadot, J.L. Aider, J.E. Wesfried, Bluff body drag reduction by extremum seeking control. J. Fluids Struct. 22 (2006) 973–978.
[18] J.F. Beaudoin, O. Cadot, J.L. Aider, J.E. Wesfried, Drag reduction of a bluff body using adaptive control methods. Phys. Fluids 18 (8) (2006) 085107.
[19] K. Roussopoulos, Feedback control of vortex shedding at low Reynolds number. J. Fluid Mech. 248 (1993) 267–296.
[20] E.A. Gillies, Multiple sensor control of vortex shedding. AIAA J 39 (4) (2000) 748–750.
[21] D.S. Park, D.M. Ladd, E.W. Hendricks, Feedback control of von Karman vortex shedding behind a circular cylinder at low Reynolds numbers. Phys. Fluids 6 (1994) 2390–2405.
[22] M.D. Gunzburger, H.C. Lee, Feedack control of vortex shedding. Trans. ASME J. Appl. Mech. 63 (1996) 828–835.
[23] C. Min, H. Choi, Suboptimal feedback control of vortex shedding at low reynolds numbers. J. Fluid Mech. 401 (1999) 123–156.
[24] P.T. Tokumaru, P.E. Dimotakis, Rotary oscillation control of a cylinder wake. J. Fluid Mech. 224 (1991) 77–90.
[25] H.M. Warui, N. Fujisawa, Feedback control of vortex shedding from a circular cylinder by cross-flow cylinder oscillations. Exp. Fluids 21 (1996) 49–56.
[26] J.E. Ffowcs Williams, B.C. Zhao, The active control of vortex shedding. J. Fluids Struct. 3 (1989) 115–122.
[27] N. Fujisawa, G. Takeda, Flow control around a circular cylinder by internal acoustic excitation. J. Fluids Struct. 17 (2003) 903–913.
[28] C.W. Rowley, D.R. Williams, Dynamics and control of high-Reynolds number flow over cavities. Ann. Rev. Fluid Mech. 38 (2006) 251–276.
[29] Z. Chen, Fan, B. Zhou, N. Aubry, Control of vortex shedding behind a circular cylinder using electromagnetic forces. Mod. Phys. Lett. B 19 (28/29) (2005) 1627–1630.
[30] O. Posdziech, R. Grundmann, Electromagnetic control of seawater flow around circular cylinders. Eur. J. Mech. B Fluids 20 (2001) 255–274.
[31] L.N. Cattafesta, S. Garg, D. Shukla, Development of piezoelectric actuators for active flow control. AIAA J 39 (8) (2001).
[32] N. Kurimoto, Y. Suzuki, N. Kasagi, Active control of lifted diffusion flumes with arrayed micro actuators. Exp. Fluids 39 (2005) 995–1008.
[33] J. Gerhard, M. Pastoor, R. King, B.R. Noack, A. Dillmann, M. Morzyński, G. Tadmor, Model-based control of vortex shedding using low-dimensional Galerkin models, AIAA-Paper, 2003-4261 (2003).
[34] J. Lumley, P. Blossey, Control of turbulence. Ann. Rev. Fluid Mech. 30 (1998) 311–327.
[35] S.V. Patankar, Numerical Heat Transfer and Fluid Flow. Hemisphere, Washington, DC, 1980.
[36] Fluent 6.2 User's Guide. Fluent Inc., 2006.
[37] H.J. Ferziger, M. Peric, Computational Methods for Fluid Dynamics. Springer, 1999.
[38] M. Van Dyke, An Album of Fluid Motion. Parabolic Press, 1988.
[39] A.E. Perry, M.S. Chong, T.T. Lim, The vortex shedding process behind two-dimensional bluff bodies. J. Fluid Mech. 116 (1982) 77–90.
[40] M.S. Engelman, Md-Ali jamina, Transient flow past a circular cylinder: a bench mark solution. Int. J. Numer. Met. Fluids 11 (7) (1990) 985–1000.
[41] S. Kang, H. Choi, S. Lee, Laminar flow past a rotating circular cylinder. Phys. Fluids 11 (1999) 3312–3321.
[42] M. Behr, J. Liou, R. Shih, T.E. Tezduyar, Vorticity - stream function formulation of unsteady incompressible flow past a cylinder: sensitivity of the computed flow field to the location of the outflow boundary. Int. J. Numer. Met. Fluids 12 (1991) 323–342.
[43] B. Sharman, F.S. Lien, L. Davidson, C. Norberg, Numerical prediction of low Reynolds number flows over two tandem circular cylinders. Int. J. Numer. Met. Fluids 47 (5) (2005) 427–447.
[44] S.K. Jordan, J.E. Fromm, Oscillating drag, lift, torque on a circular cylinder in a uniform flow. Phys. Fluids 15 (3) (1972) 371–376.
[45] A. Burbeau, P. Sagaut, Simulation of a viscous compressible flow past a circular cylinder with higher-order discontinuous Galerkin methods. Comput. Fluids 31 (2002) 867–889.
[46] O. Posdziech, R. Grundmann, A systematic approach to the numerical calculation of fundamental quantities of the two-dimensional flow over a circular cylinder. J. Fluids Struct. 23 (2007) 479–499.
[47] Private communication from Prof. T. Yokomizo.

Please cite this article in press as: S. Muddada, B.S.V. Patnaik, An active flow control strategy for the suppression of vortex structures behind a circular cylinder, European Journal of Mechanics B/Fluids (2009), doi:10.1016/j.euromechflu.2009.11.002